energies

MDPI

Article

Numerical Modeling of the Wave Energy Propagation in the Iberian Nearshore

Eugen Rusu

Department of Mechanical Engineering, Faculty of Engineering, "Dunărea de Jos" University of Galati, 47 Domneasca Street, 800008 Galati, Romania; Eugen.Rusu@ugal.ro; Tel.: +40-740-205-534

Received: 30 March 2018; Accepted: 13 April 2018; Published: 18 April 2018

Abstract: In the present work the wave energy propagation patterns in the western side of the Iberian nearshore were evaluated. This assessment takes into account the results provided by a wave modelling system based on spectral phase averaged wave models, which considers subsequent computational domains with increasing resolution towards the coast. The system was previously validated against both in situ measurements and remotely sensed data. Moreover, several data assimilation techniques were implemented as well. In this way, the reliability of the wave predictions was significantly increased. Although extended wave hindcasts have already been carried out close to the Iberian coast of the Atlantic Ocean, including wave energy assessments, they might not be completely accurate because of recent changes in the dynamics of the ocean and coastal wave climate. Thus, the present work considers wave nowcasts that correspond to the most recent and relevant wave energy propagation patterns in the targeted coastal environment. In order to perform this analysis, four different computational levels were considered. The first level corresponds to the sub oceanic domain and it is linked directly to the oceanic wave model, which is implemented over the entire North Atlantic Ocean. The second is related to the coarser computational domains of the coastal areas, while the third relates to the high-resolution domains. These three levels are defined as spherical coordinates (longitude, latitude). Finally, the last computational level includes some coastal areas which have the highest spatial resolution, defined considering the Cartesian coordinates. Moreover, for each level several computational domains have been considered. This work illustrates the most recent and significant wave transformation and energy propagation patterns corresponding to 18 computational domains with various resolutions in the western Iberian coastal environment.

Keywords: Iberian nearshore; coastal areas; wave power; numerical modeling; Simulating waves nearshore (SWAN)

1. Introduction

All over the world, ambitious objectives for low carbon energy sources and climate change policy have been set. The European Union (EU) targets aim to increase the share of renewable energy to 20% by 2020 and at least to 27% by 2030 [1]. In order to achieve such targets, significant investments in the area of renewable energy, including the acceleration of research and innovation (R & I), are expected. Nowadays, coastal environments represent the most challenging areas for renewable energy extraction. This is because the nearshore has huge energy potential, especially with regard to offshore wind, waves and tides. The most spectacular evolutions can be seen in the area of offshore wind. Thus, both fixed wind turbines and floating platforms are being quickly implemented and they have become commercially efficient [2,3]. Most of the advances in offshore wind energy is due to the high performance and innovative design of large wind turbines (WT). The major challenge in offshore renewable energy is the achievement of a significant reduction in the levelized cost of energy (LCOE). From this perspective, a revolutionary idea in the wind industry is represented by

the multi-rotor concept. This means having more rotors on a single support structure, which avoids the upscaling disadvantages of the unit turbine and at the same time facilitates the benefits of large unit capacities. An analysis using a cost model compared 20 MW multi-rotor systems to 10 MW reference turbines in a specified 500 MW wind farm, shows major benefits for this concept [3]. According to this analysis, the multi-rotor system achieved 7.2 ct€/kWh with a cost reduction of about 33% relative to the LCOE of the reference turbines.

The very high dynamics of offshore wind has also encouraged the development of other technologies for renewable energy extraction in the marine environment. In this context, the EU SET-Plan (European Union Strategic Energy Technology Plan) [4] sets the LCOE targets for tidal streams as 15 ct€/kWh by 2025 and 10 ct€/kWh by 2030, while for wave energy there is a five-year shift in the LCOE target, which means 15 ct€/kWh by 2030 and 10 ct€/kWh by 2035. Nevertheless, it is expected that the advances in the offshore wind industry in relation to wave energy extraction technologies will have a great impact. This is because it creates the possibility of collocation of wave devices in the vicinity of wind farms. Such an approach has three major advantages: (a) The grid connection and other infrastructure costs that have already been completed for the wind farm can also be used by the wave farm. Thus, a substantial capital expenditure (CAPEX) reduction is expected. (b) Many parts of the maintenance operations for WTs and wave energy converters (WECs) can be combined. In this way a substantial operational expenditure (OPEX) reduction is also expected. (c) The wave farm could be used as an obstacle to protect the wind farm, or alternatively the wave farm may provide coastal protection. Thus, although wave extraction technologies are not yet considered to be mature, significant advances are expected in the near future.

Wave energy is abundant, since there are large areas of the coastal environment with significant wave power potential. Furthermore, it has higher density and predictability than wind or solar energy. Thus, although the technologies for wave energy extraction are not yet fully evolved, significant advances are expected in the near future and various types of wave energy converters are being developed (see for example [5,6]). A very important issue in increasing the efficiency of wave energy conversion is related to the development of more advanced power take-off (PTO) systems, through which the wave power is transformed into electric power, and for this reason a lot of theoretical and experimental research is being carried out in this area [7,8].

Therefore, the objective of the present work is to provide an updated picture of the wave energy propagation patterns in the western side of the Iberian nearshore. There are two reasons for this choice. First, this coastal environment is very attractive for wave energy developers [9–11] and any new study related to the wave energy patterns here should be of considerable interest. In 2008, in the coastal environment north of Porto, the world's first multiple machine wave power project was installed, known as the Aguçadoura Wave Farm. This was based on three first generation Pelamis type wave energy converters, with a total capacity of 2.25 MW. The farm first generated electricity in July 2008 but was taken offline in November 2008.

The second reason is related to the fact that the coastal wave climate may change and as a result new propagation patterns, either global or/and local, may occur [12]. Thus, although there are many studies concerning the wave propagation patterns in this coastal environment, some of them are focused only on the evaluation of the wave energy patterns in the Spanish [13–16] or in the Portuguese [17–19] nearshores. Furthermore, evaluations related to the expected performances of the current state-of-the-art wave energy converters in the Iberian coastal environment have been carried out [20–22]. The results look promising and if we compare the west Iberian nearshore with some of the most energetic locations in the Mediterranean Sea where similar investigations are currently being performed, see for example [23–25], it can be considered as one of the most attractive European coastal environments for the implementation of marine energy farms in the future.

2. Materials and Methods

2.1. Theoretical Background of the Spectral Wave Models

The wave models based on the spectrum concept integrate an advection type equation that gives the propagation of the wave spectrum in a space defined by five dimensions: time, geographical and spectral spaces [26,27]:

$$\frac{DN}{Dt} = \frac{S}{\sigma}. \tag{1}$$

The spectrum that is considered in the great majority of spectral wave models is the action density spectrum (N), rather than the energy density spectrum. This is because in the presence of the currents action, density is conserved while energy density is not. The concept of wave action was introduced by Bretherton and Garret [28], and the action density is equal to the energy density (E) divided by the relative frequency (σ). S from the right-hand side of Equation (1) represents the source terms. The radian relative frequency is related to the wave number (k) by the dispersion relationship:

$$\sigma^2 = gk \tanh(kd), \tag{2}$$

where g is the acceleration of gravity and d the water depth. In the presence of currents, the absolute radian frequency (ω) is given by the usual Doppler shift:

$$\omega = \sigma + \vec{k}\vec{U}, \tag{3}$$

where $\vec{k}$ is the wave number vector and $\vec{U}$ is the current velocity.

For large scale applications the governing Equation (1) is expressed for the geographical space in spherical coordinates, longitude (λ) and latitude (φ), while the spectral space is defined by the relative frequency (σ) and the wave direction (θ):

$$\frac{\partial N}{\partial t} + \frac{\partial}{\partial \lambda}\dot{\lambda}N + \frac{1}{\cos\varphi}\frac{\partial}{\partial \varphi}\dot{\varphi}N\cos\varphi + \frac{\partial}{\partial \sigma}\dot{\sigma}N + \frac{\partial}{\partial \theta}\dot{\theta}N = \frac{S}{\sigma}, \tag{4}$$

For coastal applications the Cartesian coordinates (x) and (y) are mostly used and the action balance equation in this case becomes:

$$\frac{\partial N}{\partial t} + \frac{\partial}{\partial x}\dot{x}N + \frac{\partial}{\partial y}\dot{y}N + \frac{\partial}{\partial \sigma}\dot{\sigma}N + \frac{\partial}{\partial \theta}\dot{\theta}N = \frac{S}{\sigma} \tag{5}$$

The left side of the action balance Equations (1), (4) or (5) is the kinematic part which reflects the action propagation in the space with fifth dimensions accounting also for phenomena as wave diffraction or refraction. On the right-hand side the source (S) is expressed in terms of energy density. In deep water, three components are significant. They correspond to the atmospheric input, nonlinear quadruplet interactions and whitecapping dissipation. Besides these three terms, in shallow water additional terms corresponding to phenomena such as bottom friction, depth induced wave breaking or triad nonlinear wave–wave interactions may play an important role and the total source becomes:

$$S = S_{in} + S_{nl} + S_{dis} + S_{bf} + S_{br} + S_{tr} + \cdots. \tag{6}$$

In spectral wave models, the wave power components (expressed in W/m, i.e., energy transport per unit length of wave front), are computed with the relationships [29]:

$$P_x = \rho g \iint c_x\, E(\sigma,\theta) d\sigma\, d\theta \tag{7}$$

$$P_y = \rho g \iint c_y E(\sigma,\theta) d\sigma\, d\theta$$

In the above equation x, y are the problem coordinate system and c_x, c_y are the propagation velocities of wave energy in the geographical space (absolute group velocity components) defined as:

$$(c_x,\ c_y) = \frac{d\vec{x}}{dt}. \tag{8}$$

The absolute value of the energy transport (denoted also as wave power) will be:

$$P = \sqrt{P_x^2 + P_y^2}, \tag{9}$$

2.2. Description of the Wave Prediction System

A wave prediction system based on spectral phase averaged models has been considered in the present work. The ocean forcing is provided by the wave generation model Wave Modeling (WAM) Cycle 4 [30], in an improved version that allows for two-way nesting [31]. This model covers the entire North Atlantic basin. Alternatively, implementation of the Wave Watch 3 (WW3) model [32] over the same generation area has also been completed [33]. For the sub oceanic scale and the coastal domains, the Simulating Waves Nearshore (SWAN) model [34] was nested in the ocean models and various computational schemes including subsequent domains with increasing resolution towards the shore were defined [35]. Furthermore, based on these schemes an operational wave prediction system was applied to the major Portuguese harbors [36], providing nowcasts and 3-day forecasts. In this system the Fifth-Generation US National Center for Atmospheric Research (NCAR)/Penn State Mesoscale Model (MM5) model [37] is used for providing high resolution wind fields. The MM5 model is based on meteorological fields provided by the US National Oceanic and Atmospheric Administration (NOAA) Atmospheric Model Global Forecast System (GFS). The model allows for a broad set of meteorological fields at different scales and with the desired temporal resolution.

It should be noted at this point that the WAM model was mainly utilized in the wave modeling system used in the present work. WW3 was used only as a backup and it runs in parallel with WAM in some of the more sensitive cases, for example in the generation of the high energy storms in the North Atlantic Ocean and their impact in the Iberian nearshore. In general, the results provided by the two models are consistent [33], although the WAM version considered, was intensively tested and calibrated for this particular coastal environment and appears to provide slightly more reliable results.

In the present work, four different SWAN computational levels are considered. The first level is related to the sub-oceanic scale and represents the link between the ocean models and the coastal domains. Three different SWAN domains are considered at this level and their characteristics are presented in Table 1. In this table $\Delta\lambda$ and $\Delta\varphi$ represent the spatial resolution, Δt the time resolution, nf number of frequencies, $n\theta$ number of directions, $n\lambda$ number of grid points in longitude, $n\varphi$ number of grid points in latitude and np is total number of grid points. These domains are denoted as wave drivers (D), (D1) covers the northwestern part of the Iberian Peninsula, (D2) is related to the entire western Iberian coastal environment and (D3) covers the Portuguese continental nearshore. For all these driver domains the spatial resolution is 0.05° for longitude and also 0.05° for latitude for (D1) and (D3), while for (D2) the resolution in latitude is 0.1°. Figure 1 illustrates the geographical space of (D1) in a bathymetric map, Figure 2a shows the domain (D2) and Figure 2b shows the geographical space of (D3).

Table 1. Characteristics of the driver computational domains defined for the Simulating Waves Nearshore model (SWAN) simulations in the western Iberian nearshore.

Driver Domains	$\Delta\lambda \times \Delta\varphi$	Δt (min)	nf	$n\theta$	$ng\lambda \times ng\varphi = np$
D1-Northern	0.05° × 0.05°	10 non-stat	24	24	141 × 121 = 17,061
D2-Western	0.05° × 0.1°	10 non-stat	24	24	101 × 101 = 10,201
D3-Portuguese	0.05° × 0.05°	10 non-stat	24	24	81 × 121 = 9801

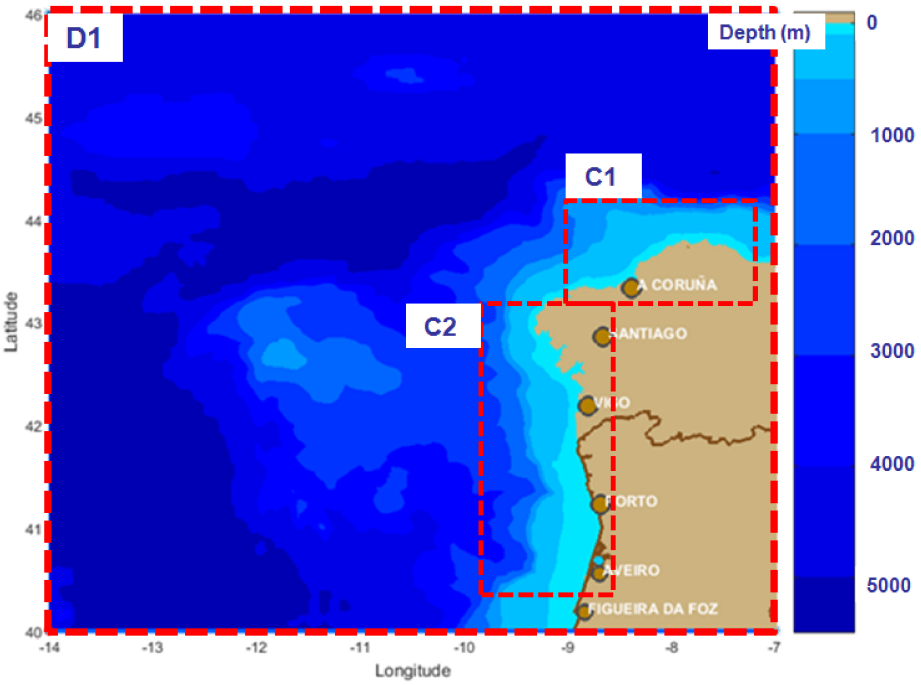

Figure 1. The northern wave driver and the subsequent coastal computational domains.

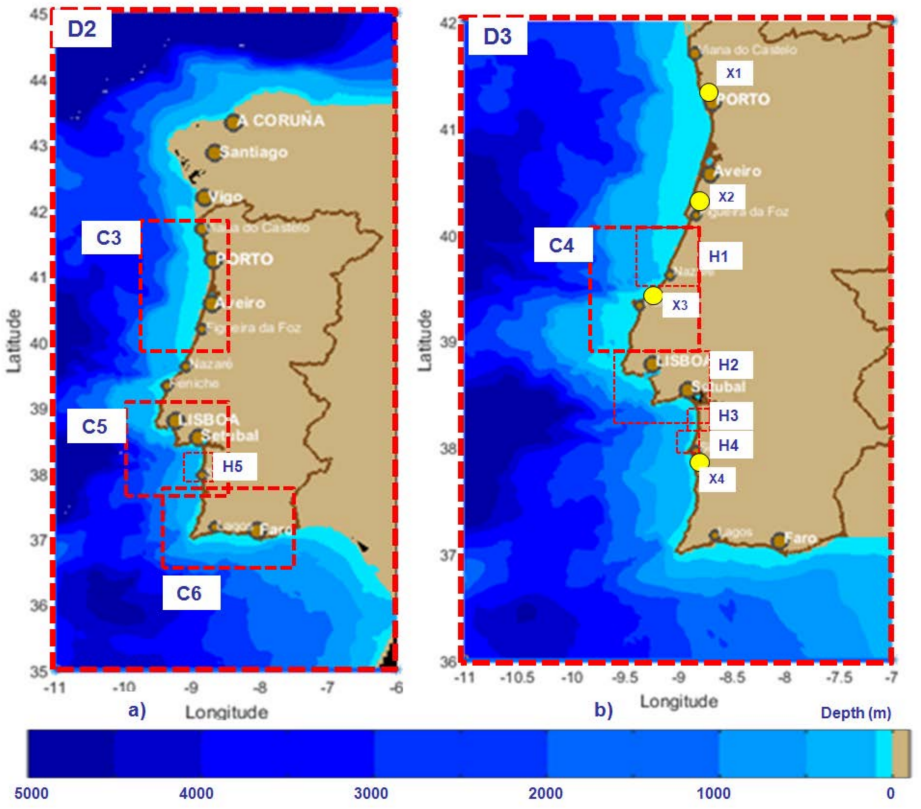

Figure 2. The Iberian (**a**) and the Portuguese (**b**) wave drivers and the subsequent computational domains corresponding to the computational levels: coastal, high resolution and Cartesian, respectively.

Six SWAN coastal domains (denoted as the C domains) are considered in the present work. These are (C1) in the north, (C2) and (C3) in the northwest, (C4) and (C5) in the center, and (C6) in

the south. Most of these domains have a resolution in the geographical space of 0.02°. However, for (C1), (C2) and (C3) the resolution in the direction normal to the mean coastline direction is 0.01°. The characteristics of the coastal domains are presented in Table 2. It should be noted that the choice of defining the resolution in the geographical space is also linked with the computational effectiveness. The coastal SWAN domains (C1) and (C2) are illustrated in Figure 1, (C3), (C5) and (C6) in Figure 2a and (C4) in Figure 2b.

Table 2. Characteristics of the coastal coarse computational domains defined for the SWAN simulations in the Iberian nearshore.

Coastal Domains	$\Delta\lambda \times \Delta\varphi$	Δt (min)	nf	$n\theta$	$ng\lambda \times ng\varphi = np$
C1-Northern	0.02° × 0.01°	10 non-stat	24	36	101 × 101 = 10,201
C2-North Western 01	0.01° × 0.02°	10 non-stat	24	36	101 × 141 = 14,241
C3-North Western 02	0.01° × 0.02°	10 non-stat	24	36	101 × 101 = 10,201
C4-Central 01	0.02° × 0.02°	10 non-stat	24	36	76 × 91 = 6916
C5-Central 02	0.02° × 0.02°	10 non-stat	24	36	63 × 76 = 4788
C6-Southern	0.02° × 0.02°	10 non-stat	24	36	111 × 76 = 8436

Furthermore, five SWAN high-resolution domains (denoted as the H domains) are considered in the present work. They have spatial resolutions in the range 0.001°–0.01° and these are: (H1) corresponding to the nearshore area of Peniche, (H2) in the vicinity of Lisbon, (H3) is the Pinheiro da Cruz nearshore, south of the Portuguese city of Setubal, (H4) the nearshore area located in the north of the Sines port, and (H5) the nearshore area centered on the port of Sines. The characteristics of the high-resolution SWAN domains are presented in Table 3. In Figure 2a the (H5) domain is illustrated, while Figure 2b shows the geographical spaces corresponding to all the other high-resolution computational domains (H1, H2, H3 and H4).

Table 3. Characteristics of the high-resolution computational domains considered for the SWAN simulations in the western Iberian nearshore.

High Resolution Domains	$\Delta\lambda \times \Delta\varphi$	Δt (min)	nf	$n\theta$	$ng\lambda \times ng\varphi = np$
H1-Peniche	0.01° × 0.01°	10 non-stat	30	36	91 × 81 = 7371
H2-Lisbon	0.005° × 0.01°	10 non-stat	30	36	91 × 81 = 7371
H3-Pinheiro da Cruz	0.001° × 0.0025°	10 non-stat	30	36	91 × 81 = 7371
H4- Sines North	0.002° × 0.003°	10 non-stat	30	36	91 × 81 = 7371
H5-Sines	0.005° × 0.005°	10 non-stat	30	36	101 × 101 = 10,201

Finally, four Cartesian SWAN domains have also been considered. They have spatial resolutions in the range 25–100 m and they are denoted as: (X1) in the vicinity of the Leixoes harbor, close to the Portuguese city of Porto, (X2) related to the nearshore area of Figueira da Foz, (X3) the nearshore area of Obidos in the central part of continental Portugal, and (X4) in the vicinity of the Sines harbor, south of Lisbon [38]. The characteristics of the Cartesian SWAN domains are presented in Table 4, while the corresponding geographical spaces are illustrated in Figure 2b, being represented with yellow circles.

Table 4. Characteristics of the Cartesian computational domains considered for the SWAN simulations in the west Iberian nearshore.

Cartesian Domains	$\Delta x \times \Delta y$ (m)	Δt (min)	nf	$n\theta$	$ngx \times ngy = np$
X1-Leixoes harbor	25 × 25	60 stat	30	36	236 × 216 = 50,976
X2-Figueira da Foz	25 × 50	60 stat	30	36	65 × 106 = 6890
X3-Obidos	100 × 100	60 stat	30	36	156 × 328 = 51,168
X4-Sines harbor	25 × 25	60 stat	30	36	261 × 201 = 52,461

2.3. Model System Validations and Data Assimilation

Validations were carried out for the wave modeling system using both in situ and remotely sensed measurements. The results are discussed below, considering first the model system output for various computational levels versus in situ measurements. For this, data provided by two wave rider type directional buoys were considered. One buoy was located offshore the Leixoes port (−9.0883° W/41.2033° N) and operates at a water depth of about 83 m, close to the offshore boundary of the Cartesian domain (X1). The second buoy was located offshore the Sines port (−8.9289° W/37.9211° N) and operates at approximately 97 m, close to the offshore boundary of the Cartesian domain (X4). Both are maintained by the Hydrographic Institute of the Portuguese Navy [36]. Statistical results for the simulated wave parameters against the buoy measurements are presented in Table 5 for the time interval from 5 October 2010 to 31 May 2011.

The statistical parameters presented in Tables 5 and 6 are *Bias*, root mean square error (*RMSE*), scatter index (*SI*), correlation coefficient (*r*) and symmetric slope (*S*). If X_i represents the measured values, Y_i the simulated values and n the number of observations the aforementioned parameters can be defined with the relationships:

$$X_{med} = \widetilde{X} = \frac{\sum_{i=1}^{n} X_i}{n},\ Bias = \frac{\sum_{i=1}^{n}(X_i - Y_i)}{n},\ RMSE = \sqrt{\frac{\sum_{i=1}^{n}(X_i - Y_i)^2}{n}} \tag{10}$$

$$SI = \frac{RMSE}{\widetilde{X}},\ r = \frac{\sum_{i=1}^{n}\left(X_i - \widetilde{X}\right)\left(Y_i - \widetilde{Y}\right)}{\left(\sum_{i=1}^{n}\left(X_i - \widetilde{X}\right)^2 \sum_{i=1}^{n}\left(Y_i - \widetilde{Y}\right)^2\right)^{\frac{1}{2}}},\ S = \sqrt{\frac{\sum_{i=1}^{n} {Y_i}^2}{\sum_{i=1}^{n} {X_i}^2}} \tag{11}$$

Table 5. The statistical results of the wave parameters at the buoys for the time interval 5 October 2010 to 31 May 2011. *N* represents the number of data points [36].

Parameter	Grid	*Bias*	*RMSE*	*SI*	*R*	*S*	Buoy
H_s (m)	D2	0.09	0.47	0.22	0.92	1.02	
	C3	0.12	0.40	0.18	0.95	1.04	**Leixoes**
T_{m02} (s)	D2	−0.47	1.29	0.18	0.80	0.95	***N* = 1374**
	C3	−0.55	1.06	0.15	0.86	0.93	
	D2	0.25	0.44	0.25	0.92	1.13	
	C5	0.15	0.35	0.20	0.93	1.07	
	H5	0.14	0.35	0.20	0.93	1.06	**Sines**
	D2	−0.37	1.26	0.18	0.81	0.96	***N* = 1087**
T_{m02} (s)	C5	−0.55	1.09	0.15	0.86	0.93	
	H5	−0.57	1.07	0.15	0.87	0.93	

In this table *RMSE* represents the root mean square error, *SI* the scatter index, *R* the correlation coefficient and *S* the symmetric slope. The results presented in Table 5 show that in general, the wave model predictions have good accuracy in all the computational levels considered. Closer to the coast, better accuracy in the higher resolution domains would be expected. Furthermore, in order to improve the wave predictions, an assimilation scheme for the satellite data has also been implemented at the sub oceanic levels [39]. This scheme is based on the optimal interpolation method. The basic philosophy of data assimilation (DA) is to combine the information coming from measurements with the results of the numerical models to enable the optimal estimation of the field of interest [40]. The assimilation of wave data is usually performed in terms of significant wave height (H_s). Measurements of this wave parameter are available locally (generally coming from buoys) and widespread (satellite data). The sequential methods combine all the observations falling within a particular time window and update the model solution without reference to the model dynamics. The most widely adopted DA schemes are based on instantaneous sequential procedures, such as the optimal interpolation

(OI) [41] or the successive correction method (SCM) [9]. These methods are attractive, especially due to their lower computational demands, and consequently DA schemes based on OI are widely used in wave forecasting. In fact, nowadays most of the weather prediction centers with wave modelling capabilities assimilate altimeter measurements, using various assimilation procedures based either on OI or SCM techniques.

Table 6 presents some statistical results obtained for the significant wave height values simulated with SWAN without assimilation ($H_{s\text{-}WDA}$), and obtained after the assimilation of the altimeter data ($H_{s\text{-}DA}$), against the measurements from the buoys of Leixoes and Sines in the west Iberian nearshore, considering the time interval from 5 October 2010 to 31 May 2011 [39]. As the results presented in Table 6 show, the assimilation scheme slightly improves all parameters. Also, in order to illustrate how this data assimilation scheme influences the wave field, Figure 3 presents the significant wave height scalar fields (Hs) corresponding to the time frame of 8 February 2017 without data assimilation (a) and with data assimilation (b). The satellite track, corresponding to JASON2, is also represented in Figure 2a.

Table 6. Statistical results obtained for the H_s values simulated with SWAN without assimilation ($H_{s\text{-}WDA}$), and obtained after the assimilation of the altimeter data ($H_{s\text{-}DA}$), against buoy measurements in the west Iberian nearshore, time interval from 5 October 2010 to 31 May 2011 [39].

Parameter	*MeanMes* (m)	*MeanSim* (m)	*Bias* (m)	*RMSE* (m)	*SI*	*R*	*S*	Buoy
$H_{s\text{-}WDA}$	2.15	2.23	0.08	0.47	0.22	0.91	1.03	**Leixoes**
$H_{s\text{-}DA}$		2.21	0.06	0.42	0.20	0.92	1.01	**(*N* = 1374)**
$H_{s\text{-}WDA}$	1.72	1.98	0.26	0.44	0.25	0.92	1.13	**Sines**
$H_{s\text{-}DA}$		1.95	0.23	0.39	0.23	0.93	1.12	**(*N* = 1087)**

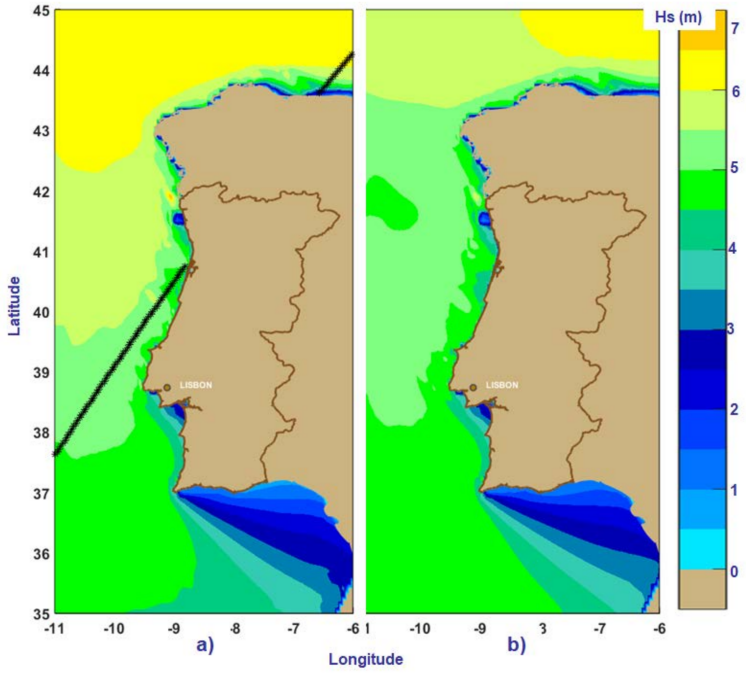

Figure 3. Significant wave height scalar fields corresponding to the time frame 8 February 2017 (**a**) results without data assimilation, the corresponding trajectory of JASON2 is also represented and (**b**) results with data assimilation.

3. Results and Discussion

Model system simulations were performed starting in October 2016 and continued until the end of 2017. Emphasis was given to the analysis of the average wintertime conditions. Since the nowcast predictions (corresponding to zero hours of each day) were found to be more accurate, and the reliability of the predictions decreased as they moved ahead into the forecast [24], the results presented next are related only to the nowcast. The physical processes activated in the SWAN simulations, corresponding to the four defined computational levels (Driver, Coastal, High Resolution and Cartesian) are presented in Table 7. In this table, *Wave* indicates the wave forcing, *Tide* the tide forcing, *Wind* the wind forcing, *Curr* the current field input, *Gen* generation by wind, *Wcap* the whitecapping process, *Quad* the quadruplet nonlinear interactions, *Triad* the triad nonlinear interactions, *Diff* diffraction process, *Bfric* bottom friction, *Set up* the wave induced set up and *Br* depth induced wave breaking. For each computational level the most relevant processes were considered. Thus, most of the deep-water processes (such as whitecapping or generation by wind) are also valid in shallow water, which is why they have been considered in all computational levels. However, for the first two levels (sub oceanic and coastal) the tide was not considered since for deep-water wave propagation the tide level does not influence the model results in any way, while building an accurate tide level matrix for a large-scale domain is a quite difficult task. In shallow water, corresponding to the high resolution and Cartesian computational domains, the tide might significantly influence the results, see for example [42] and thus the tide should be considered in the model simulations. A similar reason relates to the activation of diffraction in the high-resolution domains. Although triad nonlinear interaction is a process characteristic of shallow water, it was also activated in the coastal computational levels, because occasionally it may occur in intermediate water as well. Finally, the wave induced set up is a process that can be activated only in Cartesian coordinates.

Table 7. Physical processes activated in the SWAN simulations, corresponding to the four defined computational levels (Driver, Coastal, High Resolution and Cartesian). X—process activated, 0—process inactivated.

Input/Process / Domains	*Wave*	*Wind*	*Tide*	*Curr*	*Gen*	*Wcap*	*Quad*	*Triad*	*Diff*	*Bfric*	*Set up*	*Br*
Driver	X	X	0	0	X	X	X	0	0	X	0	X
Coastal	X	X	0	0	X	X	X	X	0	X	0	X
High Resolution	X	X	X	0	X	X	X	X	X	X	0	X
Cartesian	X	X	X	0	X	X	X	X	X	X	X	X

The results of the 15-month period of model simulations, performed in the 18 SWAN domains corresponding to the four defined computational levels, were analyzed focusing on the average wintertime conditions. It has to be noted that in these analyses, wintertime is considered the 6-month period from October to March. Some case studies that were found to be representative will be presented and discussed below.

Figure 4 illustrates some relevant wave energy propagation patterns in the northwestern side of the Iberian nearshore. These model simulations correspond to 22 October 2016, which reflects an average winter time wave energy situation. The results corresponding to the driver domain (D1) are presented in Figure 4a, while those corresponding to the coastal domains (C1) and (C2) are illustrated in Figure 4b,c, respectively. The energy propagation patterns are represented through the normalized wave power and the energy transport vectors. The mean direction of the incoming waves is about 330° (nautical convention) in the offshore, while in the nearshore this might be drastically changed due to the refraction process. Thus, in the vicinity of the Spanish city of A Corunha (see Figure 4a) the mean wave direction is about 310°, while in the nearshore of the Portuguese city Aveiro the mean wave direction is around 290°. As regards the wave power, expressed in KW/m (kilowatts over a meter of

wave front) this is normalized in the maps presented in Figure 4 and then by dividing its value by 100. For the sake of consistency, the same color bar is used for all the energy maps presented.

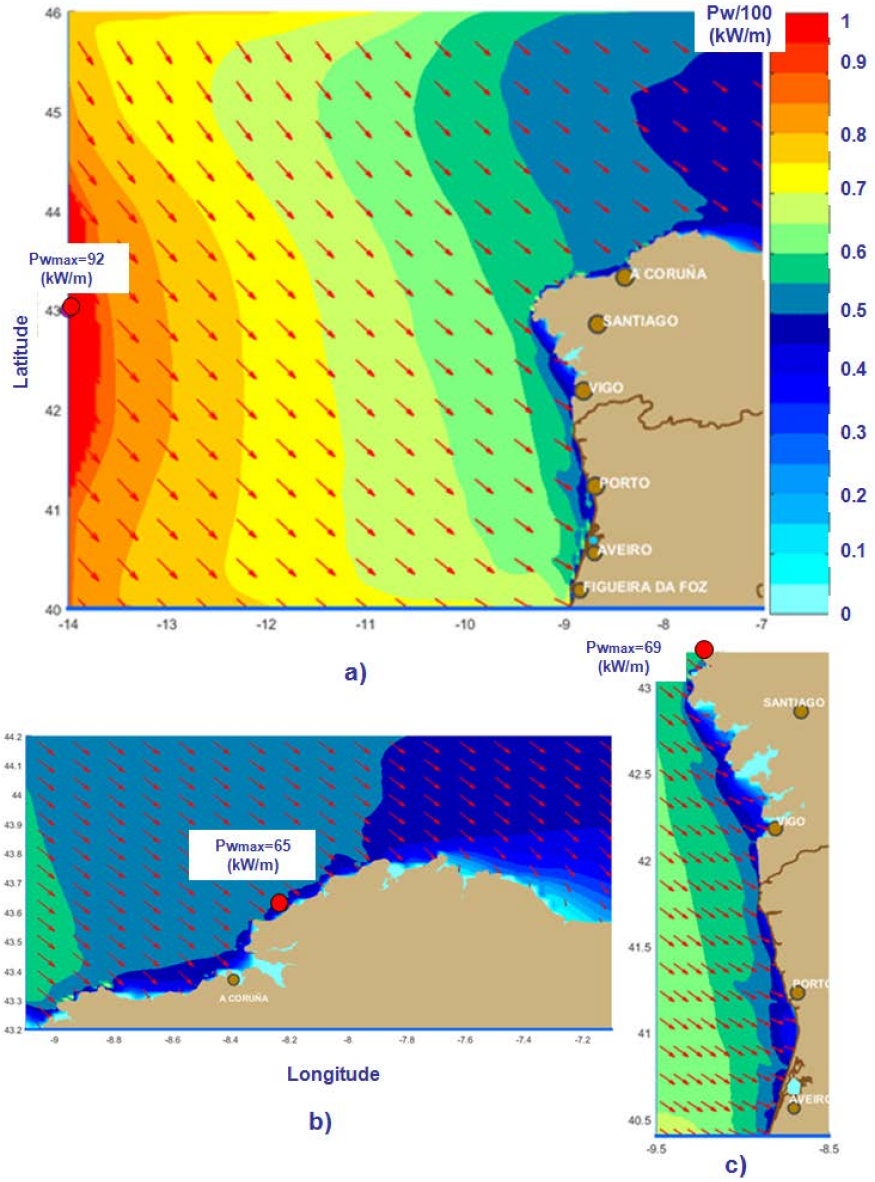

Figure 4. Normalized wave power and energy transport vectors illustrating an average winter time wave energy pattern in the northwestern Iberian nearshore. (**a**) Northern wave driver (D1); (**b**) Coastal domain (C1); (**c**) Coastal domain (C2). Model results correspond to the time frame 22 October 2016.

Some wave energy hot spots can be also identified in Figure 4b,c and they are marked with red circles in these figures. In this case study, they have estimated wave powers of 65 kW/m and 69 kW/m, respectively. These two hot spots are persistent in the sense that they occur as such in most of the simulations performed in the coastal computational domains (C1) and (C2). Figure 5 presents a relevant case study related to the wave energy propagation towards the Portuguese port of Sines, located in the central part of continental Portugal. The model results correspond to the time frame of 10 March 2017 and they show the model system focusing on wave power via the Iberian driver (D2) in Figure 5a, through the coastal central computational domain (C5) in Figure 5b and finishing with the SWAN high resolution domain (H5), in Figure 5c. The mean wave direction is this time was around 315° offshore and varies to about 300° in the vicinity of the Sines harbor. For this regular wave energy

propagation pattern, when the waves are coming from the northwest, the coastal environment south of Lisbon, including the nearshore in the vicinity of the Sines port is relatively sheltered as illustrated very clearly in all subplots belonging to Figure 5.

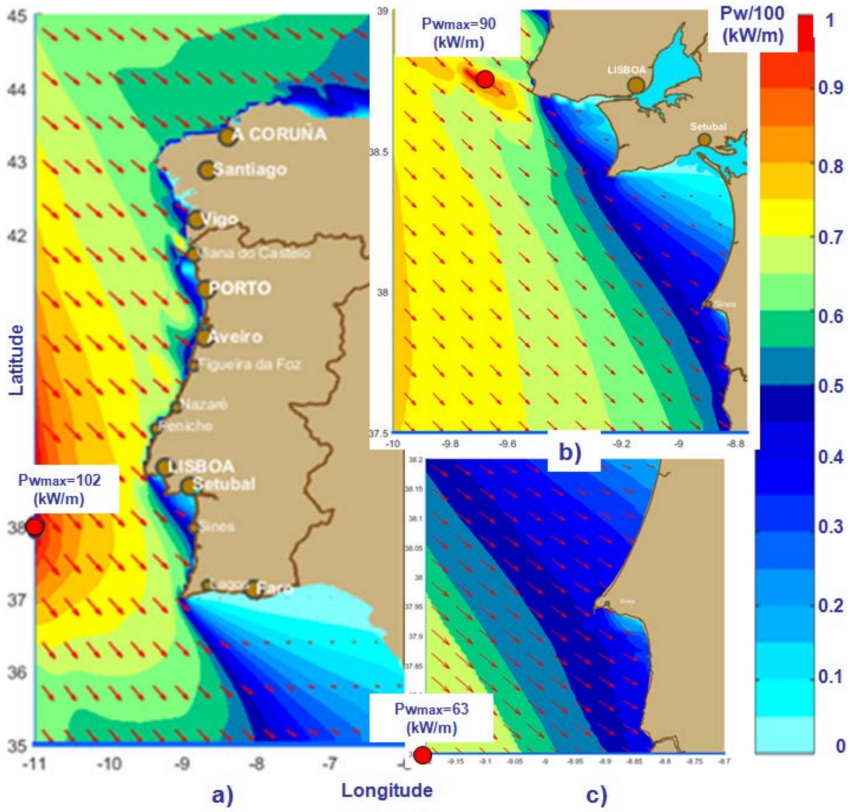

Figure 5. Wave energy propagation towards the Portuguese port of Sines. (**a**) Iberian wave driver (D2); (**b**) Coastal domain (C5); (**c**) High resolution area in the nearshore of Sines (H5). Model results correspond to the time frame 10 March 2017.

A hot spot as regards the wave energy can be also noticed in Figure 5b. This is marked with a red circle; it has an estimated wave power of 90 kW/m and is located in the vicinity of Capo DA Roca, which is the western point of continental Europe. This is also a persistent hot spot, since this coastal area is well known as being more energetic.

Figure 6 presents two different wave energy propagation patterns. Thus, Figure 6a illustrates the results for the Portuguese wave driver (D3) on 18 November 2017. This is a very common wave energy propagation pattern in the west Iberian nearshore with the waves coming from the northwest and the energy decreasing gradually from north to south. The maximum wave power is about 100 kW/m and is located offshore in the northwestern corner of the computational domain. An interesting result relates to the coastal area indicated with a red arrow. This was the location of the Aguçadora wave farm which operated in 2008 and is now one of two Portuguese pilot areas to demonstrate marine renewable energy extraction. As it can be noticed from Figure 6a, although it is not a global hot spot, there is a concentration of wave energy in this coastal environment. Figure 6b illustrates another wave energy propagation pattern in the coastal domain (C3), which corresponds to the time frame of 2 December 2017. Here, the wave energy is more focused in the central part of the Portuguese nearshore with a wave power peak of about 70 kW/m offshore the Portuguese city of Figueira da Foz. The location of the Aguçadora pilot area is also represented with a red arrow and even in such propagation conditions, enhanced local wave energy in the nearshore can be noticed.

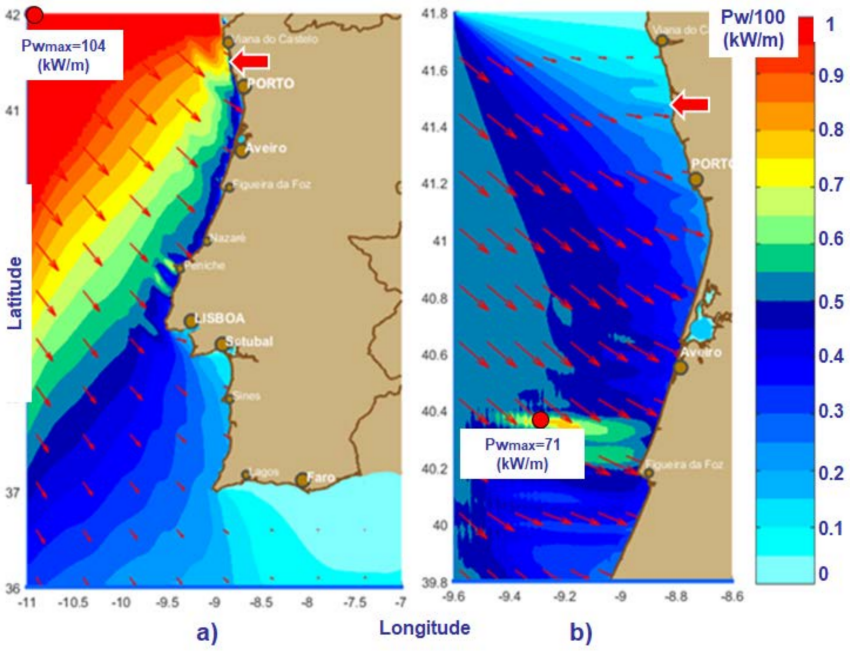

Figure 6. Wave energy propagation in the Portuguese nearshore. (**a**) Portuguese wave driver (D3), simulation corresponds to the time frame 18 November 2017; (**b**) Coastal domain (C3), simulation corresponds to the time frame 2 December 2017. The red arrow indicates one of the two Portuguese pilot areas.

Figure 7 illustrates another wave propagation pattern that corresponds to 14 October 2017, when the waves are coming from the west. Although in most cases the mean wave direction is from the northwest, there are still about 10% of situations when the dominant wave direction is from the west. Furthermore, the results of this analysis indicated a slight increase in this percentage over the last two years. Figure 7a presents the results for the coastal domain (C4). An energy peak of 78 kW/m can be noticed in the same location as in Figure 5b, which is marked with a red circle and is offshore Cabo da Roca. This demonstrates that it is a persistent hot spot. Another persistent hot spot can be seen in the nearshore of the Portuguese city of Peniche since the energy focused in this area can be also be seen in Figure 6a. Figure 7b illustrates the wave energy propagation in the southern coastal domain (C6) for the same time frame. Even though the wave propagation pattern corresponds to the waves coming from the west, the southwest of the Iberian Peninsula is sheltered and only in quite rare cases when the waves are coming from the southwest, can this nearshore be characterized by relatively high wave energy.

Figure 8 presents several wave energy propagation patterns in the high resolution computational domains. As in the previous cases presented above, they are also related to waves coming from the west. Thus, Figure 8a illustrates the wave energy propagation in the area of Peniche (H1), with the results corresponding to 18 September 2017. Again, the energy peak (89 kW/m) is located in front of Cabo da Roca. Another relevant energy peak can be noticed in the north of the computational domain in the area indicated with a red arrow, which corresponds to the second Portuguese pilot area, Sao Pedro de Moel. Figure 8b presents the wave energy propagation patterns in the nearshore of Lisbon (H2) for a simulation corresponding to the time frame 17 December 2017. The power peak (96 kW/m) also occurs in front of Cabo da Roca. Finally, Figure 8c,d present the results from the high-resolution areas Pinheiro da Cruz (H3) and North of Sines (H4), respectively. Both these results are from 19 November 2107. As it can be noticed from these figures, when the mean direction of the incoming waves is from the west, the coastal area north of Sines is no longer sheltered and an energy peak (76 kW/m for this case) occurs in the vicinity of the Sines harbor.

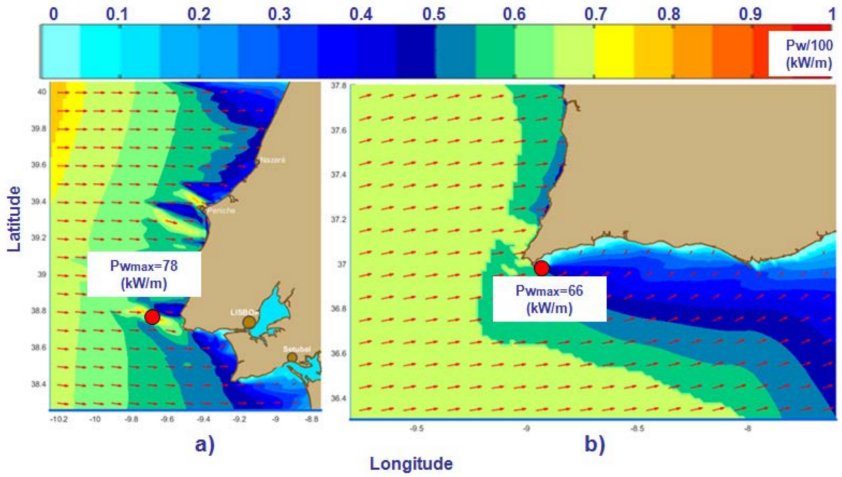

Figure 7. Wave energy propagation in the central and southern coastal domains, simulation corresponding to the time frame 14 October 2017. (**a**) Results for the central coastal domain (C4), (**b**) Results for the southern coastal domain (C6).

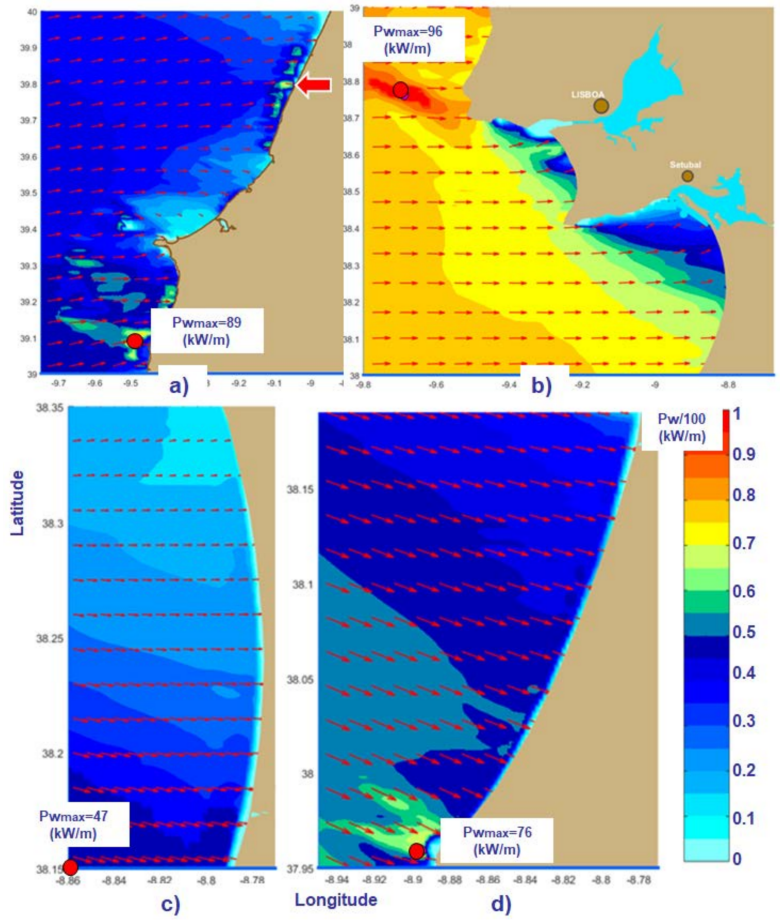

Figure 8. Wave energy propagation in the high resolution computational domains. (**a**) Peniche area (H1), simulation corresponding to the time frame 18 September 2017, the red arrow indicates one of the two Portuguese pilot areas; (**b**) Lisbon nearshore (H2), simulation corresponding to the time frame 17 December 2017; (**c**) Pinheiro da Cruz area (H3) and (**d**) North of Sines (H4), simulations corresponding to the time frame 19 November 2017.

Figures 9 and 10 illustrate case studies of wave energy propagation considering the Cartesian computational domains. Thus, Figure 9a presents a SWAN simulation corresponding to the time frame 17 September 2017 in the nearshore area Figueira da Foz (X2). The resolution of 25 m considered in the geographical space allows a good representation of the breaking process so that some very clear energy peaks that occur just before breaking are noticed in this figure, with a maximum wave power of 69 kW/m in the central part of the computational domain. Figure 9b presents a simulation in the coastal area of Obibos (X3) corresponding to the time frame 17 November 2017.

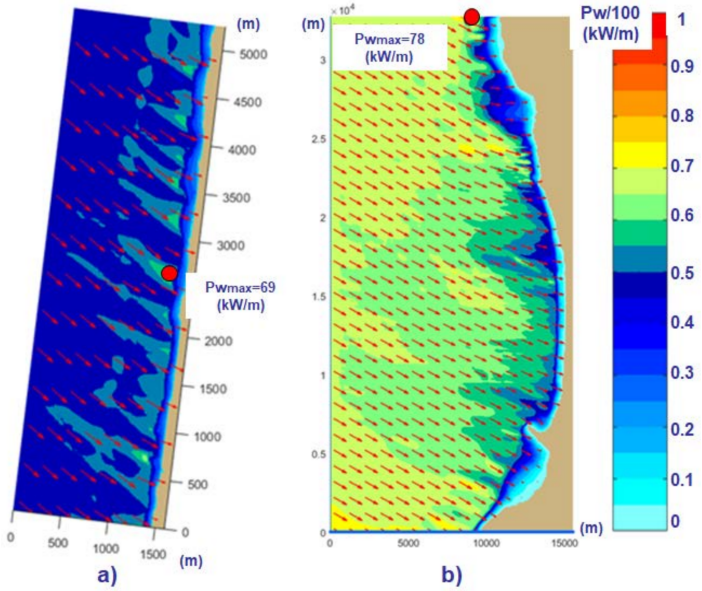

Figure 9. Wave energy propagation in the Cartesian computational domains. (**a**) Figueira da Foz (X2), simulation corresponding to the time frame 17 September 2017; (**b**) Obibos (X3), simulation corresponding to the time frame 17 November 2017.

Finally, Figure 10 presents the wave energy propagation in the vicinity of two important Portuguese harbors. These are Leixoes (X1), close to the city of Porto and Sines (X4), located south of Lisbon in the central part of the Portuguese nearshore. The results presented correspond to the time frames 17 November 2017 and 10 March 2017, respectively. No significant wave energy peaks can be seen in the vicinity of these harbors.

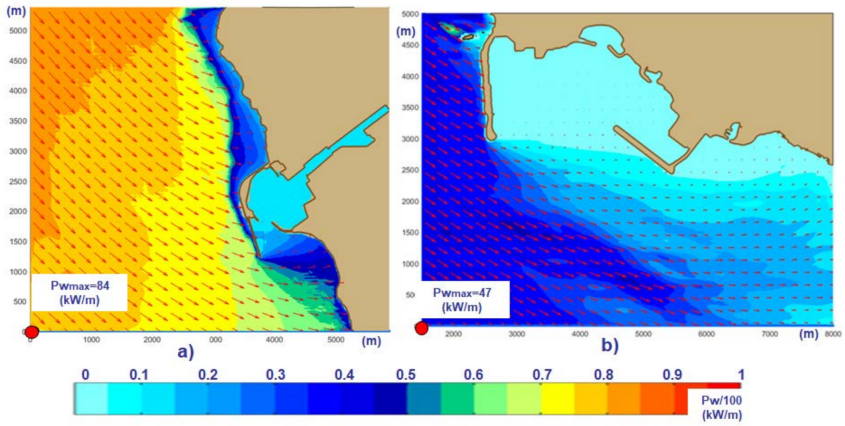

Figure 10. Wave energy propagation in the Cartesian computational domains defined close to the Portuguese harbors. (**a**) Leixoes (X1), simulation corresponding to the time frame 17 November 2017; (**b**) Sines (X4), simulation corresponding to the time frame 10 March 2017.

4. Conclusions

Starting from the fact that climate changes may induce mutations in nearshore wave energy propagation patterns, the objective of the present work is to present and analyze several recent relevant case studies that reflect the spatial distribution of the wave power in the Iberian coastal environment. For this purpose, a complex multi-level wave modelling system based on spectral phase averaged models was used. This system is focused towards the coast, with increasing spatial resolution. Furthermore, data assimilation techniques were also implemented to increase the reliability of the wave predictions, so that the results provided by this system can be considered credible. Simulations were performed for a 15-month period starting in October 2016 and finishing at the end of 2017. Some of the most relevant results are presented, considering 18 different SWAN computational domains that correspond to four geographic levels (sub oceanic, coastal, high resolution and Cartesian very high resolution).

A comparison with the results from similar studies that used the same modeling system to estimate the spatial distribution of wave energy in the west Iberian nearshore [43–46], and which were undertaken in the last 25 years, show many similar features, but also some differences. Thus, an important observation coming from the analysis of the case studies presented in this work, is that most of the wave energy hot spots already identified in the western Iberian nearshore appear to be persistent, since they were identified again in various computational domains and for various time frames. Thus, a concentration of energy waves has been very clearly identified in the nearshore in the vicinity of Cabo da Roca, the coastal environment of Peniche, the two Portuguese pilot areas and also some areas in the northern side of the Iberian Peninsula, as the nearshore gets close to the city of A Corunha. Some other general observations resulting from the analysis of the model results for the entire period considered are that, although the dominant wave direction in the western Iberian nearshore is from the northwest, the incidence of waves coming from the west appears to have increased slightly. Since the general wave energy distribution pattern in the Iberian nearshore is characterized by a gradual decrease from north to south, this new pattern may induce a global increase in the wave power in the central part of the western Iberian coastal environment. Another issue is related to the frequency and the intensity of the storms. Although the results of the model simulations performed in this 15-month period do not allow clear conclusions, they do indicate some changes in the storm dynamics. As regards the marine energy, this means careful attention should be paid to safety and survival issues.

Finally, it can be concluded that, although advances in the technologies of wave energy conversion are still needed, the high dynamics of offshore wind energy extraction will encourage momentum in the field of wave energy extraction. Furthermore, wave farms can provide protection for wind farms [47] and they can also influence coastal dynamics in various ways [48,49]. From this perspective, the present work provides a more comprehensive picture of the most recent wave energy propagation patterns in the western Iberian nearshore, which represents a very interesting coastal environment that has high potential for the future development of marine energy parks.

Acknowledgments: This work was carried out in the framework of the research project REMARC (Renewable Energy extraction in Marine environments and its Coastal impact), supported by the Romanian Executive Agency for Higher Education, Research, Development and Innovation Funding—UEFISCDI, grant number PN-III-P4-IDPCE-2016-0017. The author would like also to express his gratitude to the reviewers for their suggestions and observations that helped in improving the present work.

Conflicts of Interest: The author declares no conflict of interest.

Nomenclature

CAPEX	Capital Expenditure
DA	Data Assimilation
GFS	Global Forecast System
LCOE	Levelized Cost of Energy

EU	European Union
Hs	Significant Wave Height
MM5	Fifth-Generation Mesoscale Model
NCAR	US National Center for Atmospheric Research
NOAA	US National Oceanic and Atmospheric Administration Model
OI	Optimal Interpolation
OPEX	Operational Expenditure
Pw	Wave power
PTO	Power take-off
SCM	Successive Correction Method
SET	Strategic Energy Technology
SWAN	Simulating Waves Nearshore
WAM	Wave Modeling
WEC	Wave Energy Converter
WT	Wind Turbines
WW3	Wave Watch 3

References

1. European Commission. *Strategic Energy Technology Plan*; European Commission: Brussels, Belgium, 2014.
2. JRC. JRC Wind Energy Status Report 2016 Edition. 2016. Available online: http://publications.jrc.ec.europa.eu/repository/bitstream/JRC105720/kjna28530enn.pdf (accessed on 22 February 2018).
3. Jensen, P.H.; Chaviaropoulos, T.; Natarajan, A. LCOE Reduction for the Next Generation Offshore Wind Turbines; Outcomes from the INNWIND.EU Project. 2017. Available online: file:///C:/Users/user/Downloads/Innwind-final-printing-version.pdf (accessed on 24 February 2018).
4. SET Plan—Declaration of Intent on Strategic Targets in the Context of an Initiative for Global Leadership in Ocean Energy. 2016. Available online: https://setis.ec.europa.eu/system/files/integrated_set-plan/declaration_of_intent_ocean_0.pdf (accessed on 24 February 2018).
5. Zhang, X.; Yang, J. Power capture performance of an oscillating-body WEC with nonlinear snap through PTO systems in irregular waves. *Appl. Ocean Res.* **2015**, *52*, 261–273. [CrossRef]
6. Zhang, X.; Lu, D.; Guo, F.; Gao, Y.; Sun, Y. The maximum wave energy conversion by two interconnected floaters: Effects of structural flexibility. *Appl. Ocean Res.* **2018**, *71*, 34–47. [CrossRef]
7. Rezanejad, K.; Soares, C.G.; López, I.; Carballo, R. Experimental and numerical investigation of the hydrodynamic performance of an oscillating water column wave energy converter. *Renew. Energy* **2017**, *106*, 1–16. [CrossRef]
8. Liu, Z.; Han, Z.; Shi, H.; Yang, W. Experimental study on multi-level overtopping wave energy convertor under regular wave conditions. *Int. J. Nav. Archit. Ocean Eng.* **2017**, in press. [CrossRef]
9. Rusu, L.; Onea, F. The performance of some state-of-the-art wave energy converters in locations with the worldwide highest wave power. *Renew. Sustain. Energy Rev.* **2017**, *75*, 1348–1362. [CrossRef]
10. Veigas, M.; López, M.; Iglesias, G. Assessing the optimal location for a shoreline wave energy converter. *Appl. Energy* **2014**, *132*, 404–411. [CrossRef]
11. Bernardino, M.; Guedes Soares, C. Evaluating marine climate change in the Portuguese coast during the 20th century. In *Maritime Transportation and Harvesting of Sea Resources*; Guedes Soares, C., Teixeira, A.P., Eds.; Taylor & Francis Group: London, UK, 2018; pp. 1089–1095.
12. Iglesias, G.; Carballo, R. Wave energy and nearshore hot spots: The case of the SE Bay of Biscay. *Renew. Energy* **2010**, *35*, 2490–2500. [CrossRef]
13. Iglesias, G.; Carballo, R. Offshore and inshore wave energy assessment: Asturias (N Spain). *Energy* **2010**, *35*, 1964–1972. [CrossRef]
14. Iglesias, G.; Carballo, R. Wave energy potential along the death coast (Spain). *Energy* **2009**, *34*, 1963–1975. [CrossRef]
15. Iglesias, G.; Carballo, R. Wave energy resource in the Estaca de Bares area (Spain). *Renew. Energy* **2010**, *35*, 1574–8154. [CrossRef]

16. Rusu, E.; Soares, C.G. Wave energy assessments in the coastal environment of Portugal continental. In Proceedings of the 27th International Conference on Offshore Mechanics and Arctic Engineering, Estoril, Portugal, 15–20 June 2008; Volume 6, pp. 761–772.
17. Rusu, L.; Pilar, P.; Soares, C.G. Reanalysis of the wave conditions on the approaches to the Portuguese port of Sines. In *Maritime Transportation and Exploitation of Ocean and Coastal Resources*; Taylor & Francis Group: London, UK, 2005; Volume 1, pp. 1137–1142.
18. Silva, D.; Rusu, E.; Soares, C.G. Evaluation of Various Technologies for Wave Energy Conversion in the Portuguese Nearshore. *Energies* **2013**, *6*, 1344–1364. [CrossRef]
19. Silva, D.; Martinho, P.; Soares, C.G. Wave power resources at Portuguese test sites from 11-year hindcast data. In *Renewable Energies Offshore*; Taylor & Francis Group: London, UK, 2015; pp. 113–121.
20. Carballo, R.; Sánchez, M.; Ramos, V.; Taveira-Pinto, F.; Iglesias, G. A high resolution geospatial database for wave energy exploitation. *Energy* **2014**, *68*, 572–583. [CrossRef]
21. Rusu, E.; Silva, D.; Soares, C.G. Efficiency assessments for different WEC types operating in the Portuguese coastal environment. In *Developments in Maritime Transportation and Exploitation of Sea Resources*; Taylor & Francis Group: London, UK, 2014; pp. 961–972.
22. Silva, D.; Rusu, E.; Soares, C.G. Evaluation of the expected power output of wave energy converters in the north of the Portuguese nearshore. In *Progress in Renewable Energies Offshore*; Taylor & Francis Group: London, UK, 2016; pp. 875–882.
23. Iuppa, C.; Cavallaro, L.; Vicinanza, D.; Foti, E. Investigation of suitable sites for Wave Energy Converters around Sicily (Italy). *Ocean Sci.* **2015**, *11*, 543–557. [CrossRef]
24. Iuppa, C.; Cavallaro, L.; Foti, E.; Vicinanza, D. Potential wave energy production by different wave energy converters around sicily. *J. Renew. Sustain. Energy* **2015**, *7*. [CrossRef]
25. Vicinanza, D.; Contestabile, P.; Ferrante, V. Wave energy potential in the north-west of sardinia (Italy). *Renew. Energy* **2013**, *50*, 506–521. [CrossRef]
26. Holthuijsen, H. *Waves in Oceanic and Coastal Waters*; Cambridge University Press: Cambridge, UK, 2007; p. 387.
27. Rusu, E. Strategies in using numerical wave models in ocean/coastal applications. *J. Mar. Sci. Technol.* **2011**, *19*, 58–75.
28. Bretherton, F.P.; Garrett, C.J.R. Wave trains in inhomogeneous moving media. *Proc. R. Soc. Lond. Ser. A* **1968**, *302*, 529–554. [CrossRef]
29. SWAN Team. *Scientific and Technical Documentation*; SWAN Cycle III; Department of Civil Engineering, Delft University of Technology: Delft, The Netherlands, 2017.
30. WAMDI Group. The WAM model—A third generation ocean wave prediction model. *J. Phys. Oceanogr.* **1988**, *18*, 1775–1810.
31. Gómez Lahoz, M.; Carretero Albiach, J.C. A two-way nesting procedure for the WAM model: Application to the Spanish Coast. *J. Offshore Mech. Arctic Eng.* **1997**, *119*, 20–24. [CrossRef]
32. Tolman, H.L. A third-generation model for wind waves on slowly varying, unsteady and inhomogeneous depths and currents. *J. Phys. Oceanogr.* **1991**, *21*, 782–797. [CrossRef]
33. Silva, D.; Martinho, P.; Guedes Soares, C. Modeling wave energy for the Portuguese coast. In *Maritime Engineering and Technology*; Guedes Soares, C., Garbatov, Y., Sutulo, S., Santos, T.A., Eds.; Taylor & Francis Group: London, UK, 2012; pp. 647–653.
34. Booij, N.; Ris, R.C.; Holthuijsen, L.H. A third generation wave model for coastal regions. Part 1: Model description and validation. *J. Geophys. Res.* **1999**, *104*, 7649–7666. [CrossRef]
35. Rusu, E.; Soares, C.V.; Rusu, L. Computational strategies and visualisation techniques for the wave modelling in the Portuguese nearshore. In *Maritime Transportation and Exploitation of Ocean and Coastal Resources*; Taylor & Francis: London, UK, 2005; Volume 1, pp. 1129–1136.
36. Soares, C.G.; Rusu, L.; Bernardino, M. An operational wave forecasting system for the Portuguese continental coastal area. *J. Oper. Oceanogr.* **2011**, *4*, 17–27. [CrossRef]
37. Dudhia, J. A nonhydrostatic version of the Penn State–NCAR mesoscale model: Validation tests and simulation of an Atlantic cyclone and cold front. *Mon. Weather Rev.* **1993**, *121*, 1493–1513. [CrossRef]
38. Rusu, L.; Soares, C.G. Evaluation of a high-resolution wave forecasting system for the approaches to ports. *Ocean Eng.* **2013**, *58*, 224–238. [CrossRef]

39. Rusu, L.; Soares, C.G. Impact of assimilating altimeter data on wave predictions in the western Iberian coast. *Ocean Model.* **2015**, *96*, 126–135. [CrossRef]
40. Kalnay, E. *Atmospheric Modeling, Data Assimilation and Predictability*; Cambridge University Press: Cambridge, UK, 2003; p. 341.
41. Lionello, P.; Günther, H.; Janssen, P.A.E.M. Assimilation of altimeter data in a global third-generation wave model. *J. Geophys. Res.* **1992**, *97*, 14453–14474. [CrossRef]
42. Silva, D.; Rusu, E.; Soares, C.G. High-resolution wave energy assessment in shallow water accounting for tides. *Energies* **2016**, *9*, 761. [CrossRef]
43. Rusu, E.; Guedes Soares, C. Numerical modeling to estimate the spatial distribution of the wave energy in the Portuguese nearshore. *Renew. Energy* **2009**, *34*, 1501–1516. [CrossRef]
44. Soares, C.G.; Bento, A.R.; Goncalves, M.; Silva, D.; Martinho, P. Numerical evaluation of the wave energy resource along the Atlantic European coast. *Comput. Geosci.* **2014**, *71*, 37–49. [CrossRef]
45. Silva, D.; Bento, A.R.; Martinho, P.; Soares, C.G. High resolution local wave energy modelling for the Iberian Peninsula. *Energy* **2015**, *91*, 1099–1112. [CrossRef]
46. Bento, A.R.; Martinho, P.; Soares, C.G. Wave energy resource assessment for Northern Spain from a 13-year hindcast. In *Renewable Energies Offshore*; Taylor & Francis Group: London, UK, 2015; pp. 63–69.
47. Silva, D.; Martinho, P.; Soares, C.G. Trends in the available wave power at the Portuguese pilot zone. In *Progress in Renewable Energies Offshore*; Taylor & Francis Group: London, UK, 2016; pp. 53–59.
48. Onea, F.; Rusu, E. The expected efficiency and coastal impact of a hybrid energy farm operating in the Portuguese nearshore. *Energy* **2016**, *97*, 411–423. [CrossRef]
49. Rusu, E.; Onea, F. Study on the influence of the distance to shore for a wave energy farm operating in the central part of the Portuguese nearshore. *Energy Convers. Manag.* **2016**, *114*, 209–223. [CrossRef]